EasyChair Preprint

№ 15983

Optimization of Clusters of Spherical Aluminum Nanoparticles for Enhancing the Efficiency of Thin Film Solar Cells

Sajid Ahmed Chowdhury, Abyaz Karim,
A. F. M. Afnan Uzzaman Sheikh and Mustafa Habib Chowdhury

July 3, 2025

2024 6th International Conference on Sustainable Technologies for Industry 5.0 (STI), 14-15 December, Dhaka

Optimization of Clusters of Spherical Aluminum Nanoparticles for Enhancing the Efficiency of Thin Film Solar Cells

Sajid Ahmed Chowdhury*, Abyaz Karim*, A. F. M. Afnan Uzzaman Sheikh*, and Mustafa Habib Chowdhury**
*Dept. of Electrical and Electronic Engineering, Independent University, Bangladesh, Bangladesh
Email: 2010385@iub.edu.bd, 2110366@iub.edu.bd, 2130635@iub.edu.bd, mchowdhury@iub.edu.bd

***Abstract*—This computational study analyzes the physical parameters regarding 'clusters' of spherical aluminum nanoparticles (NPs), and their role in the enhancement of light absorption and current generation in silicon thin-film solar cells (TFSCs). Plasmonic metal NPs have been known to enhance light-trapping abilities of semiconductor substrates through localized surface plasmon resonance (LSPR). The performance can be further improved by coupling NPs within clusters having different shapes or configurations to confine light within the absorbing layer. The NP clusters take on a circular arrangement, where all NPs are equidistant from the center of the cluster. The finite-difference time-domain (FDTD) method is used to calculate the initial value for short-circuit current density (J_{SC}) from different TFSCs. Due to the large number of possible configurations for the clusters, the particle swarm optimization (PSO) algorithm was deployed to search for the best possible combination of parameters to maximize J_{SC}. The other electrical parameters were recalculated by accounting for different doping concentrations and recombination of electron-hole pairs in the silicon absorbing layer. The highest value obtained for J_{SC} was 13.9 mA/cm^2 for a 10 NP cluster with sphere radius of 48 nm and cluster radius of 191 nm which showed 38.8% efficiency enhancement compared to bare Si TFSC.**

***Index Terms*—renewable energy, sustainable development, thin film solar cells, plasmonics, nanoparticles, optimization**

I. Introduction

Solar energy has an important role in sustainable development and can be classified into either photovoltaics (PVs) or concentrated solar power [1]. For the case of photovoltaics, development of thin-film solar cells (TFSCs) have been an integral step in providing energy sustainably for the forthcoming high energy demands of tomorrow. Growing global energy demands have caused total fuel usage to escalate - where the total fossil fuel consumption rose from 94,419 TWh in 2000 to 140,231 TWh in 2023, an increase of 48.5% in 23 years [2]. Press releases from the Climate Change Conference 2023, COP28 that took place in Dubai, UAE, show that an agreement has triggered the "beginning of the end" for the era fossil fuels. The consensus of 200 parties present was that it is now necessary to ameliorate climate action to meet quotas such as a global greenhouse emission reduction by 43% to confine global warming to 1.5°C [3].

Solar energy is undeniably important as an option for renewable energy. This is enforced since in many regions in Asia and Africa where wind, tidal, or hydroelectric power are impossible, yet receive abundant sunlight. Many regions in Asia especially receive abundant sunlight and prove to be a prime site for solar PV applications. Furthermore, over the course of 2010 to 2018 the cost of generating electricity using solar PVs decreased by a substantial 77%. At the same time the installed capacity for PV technology rose from 40,334 MW to 709,674 MW [1].

With the popularity of solar PV technology as a low carbon option for sustainable energy, the question of resource use minimization has been analyzed extensively; hence, TFSCs take precedence. TFSCs utilise far less material for their construction and are much lighter than their polycrystalline and monocrystalline counterparts. However, they still lag behind in terms of performance and efficiency. Various methods have been researched to improve TFSC performance, one of which is the use of plasmonic metal nanoparticles (NPs) placed on top or embedded within the absorber substrate. This process can allow well performing TFSCs to be made with abundant and low cost materials. Another advantage TFSCs possess is that the low material usage allows more efficient use of rarer materials such as gallium arsenide (GaAs), cadmium telluride (CdTe) and perovskite solar cells, allowing for higher power-to-weight ratios for potential space applications [4] [5].

This study revolves around the use of aluminum NPs placed in ring shaped clusters on top of a silicon TFSC. Al is chosen for their ability to scatter light into the Si [6]. In each cluster, spherical NPs are placed in a circular arrangement to search for well performing patterns of the NPs to be placed upon the Si. Another reason for using clusters is that light trapping and current generation can be further enhanced by the coupling of plasmonic metal NPs. By finding the optimum NP size and distance between adjacent NPs it is possible to determine the necessary physical parameters to optimize the capabilities of Si TFSCs. This optimization is done using the particle swarm optimization (PSO) algorithm to search for a global maxima [7]. Though work has been done on the use of single Al NPs, the novelty of this paper lies in the investigation of placing said NPs in a polygonal cluster and also on the use of an algorithm to optimize the device. Apart from solar cells, clusters have also been useful in sensor applications based on surface enhanced Raman scattering (SERS) [8], and photocatalysis with the help of gold nanoclusters [9].

Throughout the paper, the term "bare Si" will be used to refer to TFSCs with no NP present. To understand the

979-8-3315-3197-3/24/31.00 © 2024$IEEE$

TFSC opto-electronic performance enhancement, as compared to bare Si, a few performance parameters are used: short-circuit current density (J_{SC}), the enhancement in EM radiation absorption, i.e. optical absorption enhancement factor (AEF), absorption, open-circuit voltage (V_{OC}) and efficiency. Furthermore, optical near-field images are generated to further understand the role of clusters of NPs in enhancing the opto-electronic performance of TFSCs to draw a final conclusion in this study.

A. The "Circular Cluster"

The objective of this study is to determine how placing NPs in a specific arrangement improves solar cell performance. The circular arrangement of NPs will be referred to as "circular cluster" and the number of NPs in the cluster will be referred to as "cluster size". Fig. 1 shows the circular cluster. Here, R is the radius of the cluster and r is the radius of the NPs. The NPs are centered at the circumference of the cluster and adjacent NPs are kept equidistant from each other.

While designing the circular cluster one thing to note is that if R is smaller than a specific value compared to r, the NPs would overlap. To prevent the overlap a restriction was placed on R, where the minimum value of R depends on r and cluster size. Equation (1) was used within the simulation to place this restriction. $\phi = \frac{2\pi}{n}$ and n = cluster size.

$$R \geq \sqrt{\frac{2r^2}{1 - cos(\phi))}} \tag{1}$$

II. Materials and Methodology

A. Simulation Setup

The simulations to compute the performance parameters of the solar cell were conducted using the commercially available software Ansys-Lumerical suite. The FDTD solver uses the finite-difference time-domain numerical method to generate optical data such as J_{SC} and electron-hole pair generation rate within the Si layer and for optimization of the geometric

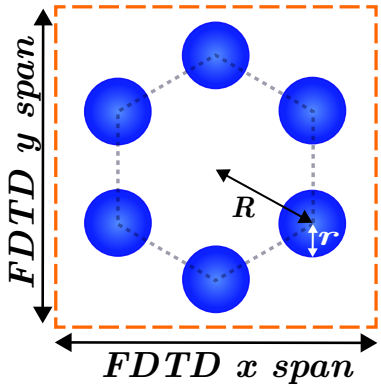

Fig. 1: A top down view of the NP cluster with the parameters labelled. The centers of the sphere are the corners of the polygon constructed, the number of sides the polygon has will be equal to the number of NPs in the cluster.

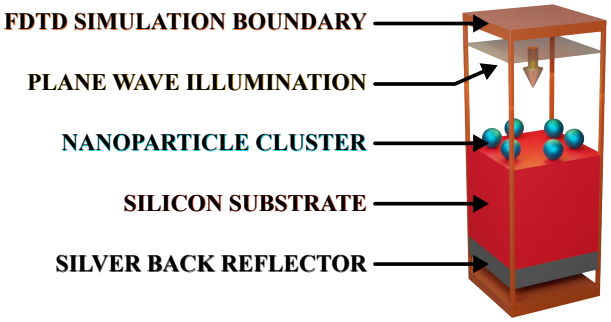

Fig. 2: 3D model depicting the setup of the simulation within FDTD. The confines of the FDTD region are pre-defined and have applied boundary conditions.

parameters of the circular cluster of NPs. The optical data generated using the FDTD method does not account for recombination. This data is then used to calculate electrical data after taking radiative, auger and trap-assisted (non-radiative) recombination into account. J_{SC}, open-circuit voltage (V_{OC}), and efficiency (η) are the electrical results computed. These electrical data have been calculated according to the equations provided by Ansys-Lumerical CHARGE solver [10]. Throughout the investigation, standard environmental conditions were maintained: solar spectrum irradiance, air mass index and temperature were kept constant at 1000 W/m^2, AM1.5G and 300 K respectively. An electromagnetic (EM) plane wave source is placed 700 nm above the absorber layer and with an incident wavelength varying from 400 nm to 1100 nm. The Si substrate of the TFSC is 500 nm thick with a 100 nm thick layer of silver underneath to act as a back reflector [6]. The back reflector reflects any transmitting radiation back into the Si absorbing layer to further increase the absorption within the absorber layer of the TFSC. According to the focus of this study, aluminum spherical NPs are placed on top of

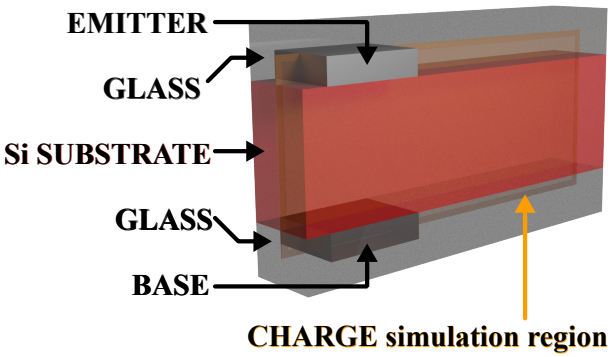

Fig. 3: 3D model depicting the CHARGE simulation to obtain necessary electrical results. The simulation takes into account of doping within the silicon substrate and recombination within the silicon substrate. CHARGE simulations are extensions of FDTD simulations as the results produced are dependent on the generation rate matrix from FDTD.

the Si substrate in a circular arrangement within the FDTD simulation region. The FDTD simulation region defines the unit that repeats to make a complete solar cell. Fig. 2 shows a 3D representation of the FDTD simulation setup.

The electrical simulation consist of extrinsic Si with a doping concentration of $4.5 \times 10^{18} cm^{-3}$ in a p-i-n configuration, where the *p*-type and *n*-type layers are 15 nm and 25 nm thick, respectively [11]. The top and bottom contacts of the solar cell were made of aluminum. To calculate electrical data a voltage sweep from 0 V to 1.5 V was done with increments of 0.05 V. The structure of TFSC is enveloped within a layer of SiO_2 to obtain accurate results [12]. The electrical simulation performed is on a 2D slice of the TFSC to save computational resources. The 2D slice is unfolded across the region to generate values of the electrical data. Fig. 3 illustrates the simulation setup of CHARGE along with its 2D slice.

B. Absorption Enhancement Factor

Absorption enhancement factor (AEF) is one of the performance parameters of the TFSC and it refers to the enhancement in absorption of EM radiation by the Si substrate compared to bare Si. The value of AEF is calculated using Equation 2. The source wavelength λ varies from 400 nm to 1100 nm and 150 wavelength points are taken within this range to calculate the AEF [6]. From Equation 3 it is apparent that the AEF of a bare TFSC at one wavelength point is equal to 1. Thus the AEF over 150 wavelength points of a bare TFSC would be 150, and any value greater than 150 would affirm an enhancement in absorption by the Si substrate with NPs present [6].

$$AEF = \int_{\lambda_1}^{\lambda_2} h(\lambda)\, d\lambda \tag{2}$$

$$h(\lambda) = \frac{\text{Absorption across Si substrate with NP cluster}}{\text{Absorption across Si substrate without NP cluster}} \tag{3}$$

C. Particle swarm optimization

Particle swarm optimization (PSO) algorithm, originally inspired by movement of flocks of birds or school of fish through space, shares a characteristic of generating a random population at first with Genetic Algorithms [13] [14]. Each point or "particle" in PSO represents a vector containing parameters, which effectively coordinate within an n-dimensional hyperspace. The positions of the particles (parameter values) are updated through velocity vectors and other variables, some of which are based in randomness. As a result, the positions of the particles can eventually converge on a global maximum value. In the context of this paper, PSO is used to optimize the different parameters of the "circular cluster" of NPs along with the distance between each repeat unit of the cluster [15].

D. FDTD region and repeating units

The FDTD region spanning its *x* span, *y* span and *z* span is the region simulated and for which the calculations are performed. The region is described as "FDTD simulation boundary" in Fig. 2. It should be noted that the cluster of NPs is supposed to repeat periodically across the surface of the substrate as shown in Fig. 4. Synonymously, the cluster is periodic with respect to the *x* and *y* axes of the space, but is not periodic with respect to the *z* axes; the upper and lower *z* boundaries have the perfectly matching layer (PML) boundary condition as a result.

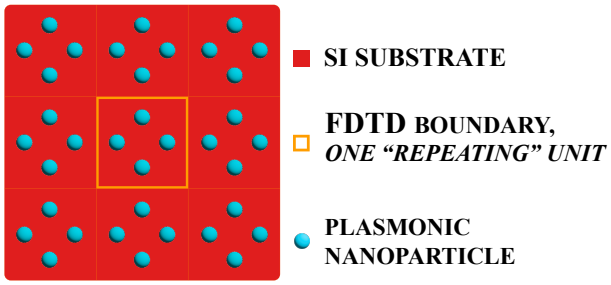

Fig. 4: Figure illustrating how the periodic *x* and *y* spans of the FDTD simulation region depicts a single unit of the TFSC that is repeated over the span of the entire TFSC.

TABLE I: PSO constraints

PSO Constraints		
	min	max
R / nm	100	250
r / nm	40	100
FDTD x span / nm	300	800
FDTD y span / nm	300	800

Thus, optimizing the *x* span and *y* span of the FDTD region in order to maximize J_{SC} allows the optimum spacing between each cluster unit cell to be determined. This will serve as valuable information for manufacturers and fabricators in order to construct TFSC of this specific design.

E. Procedure

The objective is to optimize the parameters of the circular cluster to enhance the performance of TFSCs. To achieve this the particle swarm optimization (PSO) algorithm was deployed to search for the combination of parameter values that generate the best J_{SC} from the FDTD solver. The PSO algorithm was applied for cluster sizes of 2, 4, 6, 8 and 10 NPs under the same constraints. Even number of cluster sizes allows symmetry on both the x and y axes with respect to the anti symmetric-symmetric boundary conditions for the FDTD simulation region. Table I shows the constraints placed within the algorithm to optimize the parameters.

After obtaining the results of PSO, the optical data from all the optimized clusters were used to calculate the electronic performance parameters of the TFSCs coupled with the cluster of NPs and also bare Si. For better comparison, a graph showing the absorption of radiation into the Si substrate over the 400 nm to 1100 nm wavelength range was plotted for the cluster that yielded the best result. The AEF of all the cluster sizes were compared with bare Si TFSC to understand how cluster sizes affected the enhancement. Optical near-

field images that are generated for some of the clusters show visually how placing NPs enhance light absorption.

The parameters used in optimization are R, r and the FDTD x and y spans. The algorithm was given a tolerance of 10^{-6} and a generation size of 10. Tolerance refers to the threshold value that determines when the optimization needs to stop and generation size is the number of combinations of parameters simulated in a single iteration of the PSO algorithm [16].

III. Results and Discussion

A. FDTD and Optimization

The parameters being optimized can have counteractive effects that could limit the amount of light absorbed or electricity generated within the silicon substrate. The parameters that have been analysed in this study are number of NPs in a cluster, R (distance of any NP from the center of the cluster), r (radius of a NP) and the FDTD x-y spans. For effective plasmon resonance and scattering, the aluminum NPs need to be of sufficient size and be close enough to one another. However, excessively large NPs could partially absorb the incident radiation or reflect it away from the absorbing layer of the TFSC. If NPs are too large and are not effectively spaced apart they may reflect away most light instead of allowing it to be scattered into the absorbing substrate. Moreover, for a fixed value of R, increasing the number of NPs makes the cluster resemble a ring. As a result the distance between adjacent NPs decreases, but NP do not couple effectively with respect to the TE polarization of the incident radiation.

Manual sweeps of hundreds of physical parameters (e.g., R, r, etc.) through hundreds of FDTD simulations would be highly inefficient. The PSO algorithm is utilized here to search for the global maxima and corresponding parameters. The stochastic mechanisms within PSO are highly adapted to maximizing a figure of merit given a set number of parameters. Results from PSO show that cluster containing 8 NPs with R = 230 nm and r = 64 nm provides the highest J_{SC} of 15.57 mA/cm^2 where the FDTD x and y spans are 516 nm and 563 nm, respectively. Table II shows the J_{SC} and optimized parameters of the clusters. The optical results were carried over to CHARGE solver, and the data in Table III were obtained after electrical calculations.

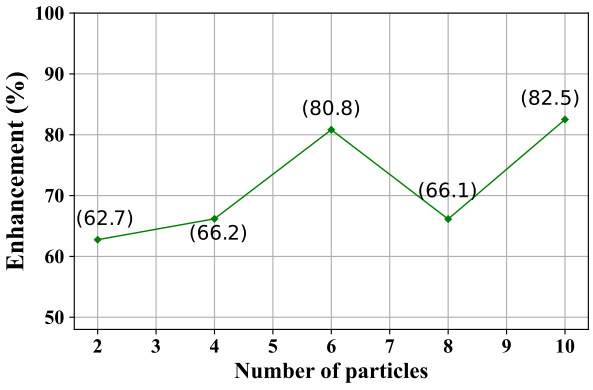

Fig. 5: Plot showing the absorption enhancement as compared to a bare Si TFSC making it evident that having clusters of NPs on top of the substrate assists in scattering light into the substrate.

TABLE II: PSO Optimized results

PSO best result			
Cluster size	**Parameters**	**Values**	**J_{SC} (mA/cm^2)**
10	R	191	14.75
	r	48	
	FDTD x	447	
	FDTD y	516	
8	R	230	15.67
	r	64	
	FDTD x	516	
	FDTD y	563	
6	R	139	14.48
	r	49	
	FDTD x	312	
	FDTD y	425	
4	R	193	14.36
	r	74	
	FDTD x	300	
	FDTD y	467	
2	R	191	14.48
	r	87	
	FDTD x	400	
	FDTD y	800	

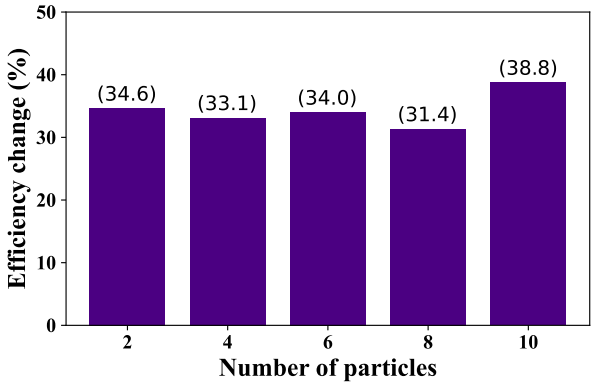

Fig. 6: Bar graph showing the increase in efficiency compared to bare Si TFSC. Following the same trend as AEF, efficiency is much higher for all the clusters relative to bare Si TFSC.

A comparison was made for the AEF relative to bare Si TFSC for the 5 clusters with optimized parameters. For increased clarity, the AEF has been compared to 150 and the amount of enhancement in absorption is expressed as a percentage. Fig. 5 shows the variation of absorption enhancement. Cluster size of 10 shows the maximum enhancement of 82.5%, which follows the same pattern as shown by the efficiency (η) comparison from electrical results in Fig. 6. It is worth noticing that the AEF increases for increasing cluster sizes, except 8. A possible explanation for this would be that for the 8-NP cluster, the pattern of the arrangement led to a larger distance between non-adjacent NPs and worse coupling with neighbouring clusters. Evidence for worse coupling with neighbouring clusters can be seen by observing left and right edges of the near-fields and referring to Fig. 4.

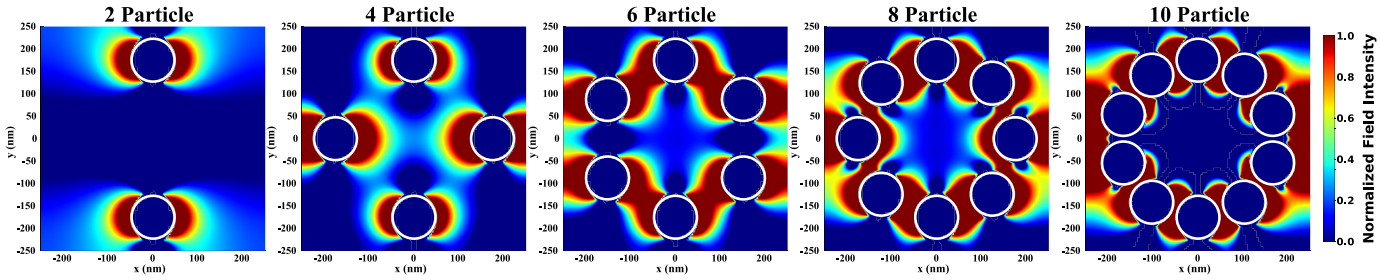

Fig. 7: Optical near-field enhancement images showing the confinement of EM field assisted by NPs coupled within the five different clusters.

TABLE III: Simulated electrical TFSC performance parameters using CHARGE

Cluster Size	0 - Bare Si	2	4	6	8	10
V_{OC} (V)	0.50	0.49	0.48	0.48	0.50	0.50
J_{SC} (mA/cm^2)	10.00	13.50	13.47	13.53	13.10	13.87
Efficiency (η %)	3.90	5.26	5.20	5.23	5.13	5.42
FF	0.78	0.79	0.81	0.81	0.78	0.78
P_{OUT} (mW/cm^2)	3.90	5.26	5.20	5.23	5.13	5.42

B. Electrical results

The electrical results are shown in Table III. Unlike optical data generated by FDTD, the electrical data generated by CHARGE shows maximum J_{SC} is generated by a cluster with 10 NPs. One possible reason for this minor discrepancy can be because FDTD calculations do not take recombination of electron-hole pairs into account. While taking the recombination into account the J_{SC} decreases as expected. This, alongside the fact that the FDTD x and y spans of the 5 different optimized clusters of NPs are different, may be the reason why cluster size of 10 yields better final results than 8.

From electrical results, the efficiency and J_{SC} follow a similar pattern, with a cluster size of 10 yielding the maximum efficiency of 5.418% which is a 38.8% increase in efficiency compared to bare Si TFSC. It is notable placing 10 NPs in a cluster provides the highest increase in efficiency, the other configurations also show marked improvements over bare Si TFSC. To understand how the efficiency of TFSCs coupled to the NPs are affected relative to bare Si TFSC, a bar graph in Fig. 6 is plotted.

Optical near-field plots in Fig. 7 show how the NPs in all the clusters confine light near the Si absorbing substrate. The red areas represent areas of near field enhancement. It is apparent that a cluster containing 10 NPs shows the best light confining capability out of the 5 cluster sizes investigated. This result aligns with the previously calculated data which showed cluster size of 10 had the highest values in most of the opto-electronic performance parameters of TFSCs like J_{SC} and efficiency. It should be noted that the area of the cluster shown in the near field images are a single repeat unit of the cluster throughout the span of the TFSC. Therefore each cluster interacts with its adjacent clusters to further enhance the confinement of EM radiation into the entire Si absorbing substrate.

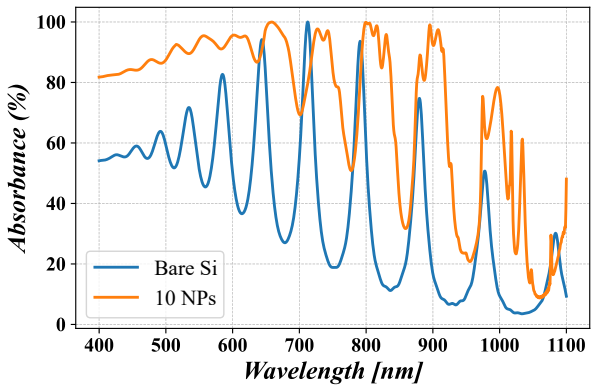

Fig. 8: Plot showing the absorption of light by a cluster containing 10 NPs across the span of source wavelength, 400nm to 1100nm. Absorption by bare Si is provided for comparison.

Lastly, the absorption of radiation into the absorber layer over the 400 nm to 1100 nm range of source wavelength is plotted. Fig. 8 shows that placing NPs within a cluster increase absorption over the entire range of wavelengths. The absorption is highest in wavelength regions of 800 nm-900 nm.

C. Nanoparticle fabrication and placement

The clusters of NPs featured in this study are an application of a 2D assembly of NPs across a surface. With the imposed conditions on the study, the analysis performed has been specific to these clusters containing 2, 4, 6, 8 and 10 NPs each. The placement of these Al spherical NPs need to be precise to achieve favourable results. Hence, the absorber layer likely needs to be templated to guide the placement of the NPs on the substrate. To guide the NPs onto their designated sites on the substrate, field-assisted manipulation can be used to ensure precision in the patterning over a large area [17]. Templated structures need to be pre-fabricated and require techniques such as electron beam lithography (EBL), which may be most appropriate given the substrate is Si [18]. The formation of the Al NPs can also be done efficiently with the use of EBL or alternatively pulsed laser ablation (PLA) [19]. The use of EBL incurs the possibility of minor distortions

in the Al NPs [19], yet should not fully limit performance enhancements as defective and imperfect NP can also provide notable improvements in efficiency [20].

IV. Conclusion

This computational study utilizes the finite-difference time-domain (FDTD) numerical method to demonstrate that placing spherical aluminum nanoparticles (NPs) in a circular arrangement forming a cluster enhances the efficiency of Si thin film solar cells (TFSCs) coupled to the clusters compared to Si TFSCs having no coupled NPs present. Within the cluster, the maximum efficiency is 5.42% (which represents ≈39% increase in efficiency compared to bare Si TFSC) shown by a cluster containing 10 NPs where the radius of the cluster is 191 nm and radius of the NPs is 48 nm. Such an arrangement yields a short-circuit current density (J_{SC}) of 13.87 mA/cm^2, open-circuit voltage (V_{OC}) of 0.50 V, fill factor (FF) of 0.79 and produces a maximum output power (P_{OUT}) of 5.42 mW/cm^2. A possible reason for the enhancement may be that clusters allow multiple NPs to undergo plasmonic coupling, thus leading to a larger surface plasmon resonance. Furthermore, the feasibility of the fabrication and placement of the NPs in a specific arrangement through processes such as electron beam lithography and pulsed laser ablation are also discussed.

Related future works will focus on a wider range of possible configurations as well as investigation of more particles within a single cluster to obtain a pattern of NPs that can provide optimal optical and electrical results. Instead of solely relying on clusters where NPs have a circular arrangement, various grids of NPs can be analyzed to see how the confinement of incident radiation (e.g. incident sunlight) can be maximized. Robustness of possible future analyses can be ensured by testing and comparing the effectiveness of different materials for the plasmonic metal NPs or even observing the coupling effect of NPs of varying morphologies. Moreover, other algorithms like Genetic Algorithm or Simulated Annealing can be utilised for the purpose of optimization to see if they can provide more efficient means to approach global maxima compared to particle swarm optimization (PSO).

Acknowledgment

The authors of this paper would like to acknowledge Independent University Bangladesh (IUB) for funding the research and for providing the necessary logistical support.

References

[1] A. O. M. Maka and J. M. Alabid, "Solar energy technology and its roles in sustainable development," *Clean Energy*, vol. 6, no. 3, pp. 476–483, Jun. 2022. [Online]. Available: https://doi.org/10.1093/ce/zkac023

[2] H. Ritchie, P. Rosado, and M. Roser, "Fossil fuels," *Our World in Data*, Jan. 2024. [Online]. Available: https://ourworldindata.org/fossil-fuels

[3] "COP28 Agreement Signals "Beginning of the End" of the Fossil Fuel Era — UNFCCC," Dec. 2023. [Online]. Available: https://unfccc.int/news/cop28-agreement-signals-beginning-of-the-end-of-the-fossil-fuel-era

[4] K. Chopra, P. Paulson, and V. Dutta, "Thin-Film Solar Cells: An Overview," *Progress in Photovoltaics - PROG PHOTOVOLTAICS*, vol. 12, pp. 69–92, Mar. 2004. [Online]. Available: https://doi.org/10.1002/pip.541

[5] Y. Li, X. Ru, M. Yang, Y. Zheng, S. Yin, C. Hong, F. Peng, M. Qu, C. Xue, J. Lu, L. Fang, C. Su, D. Chen, J. Xu, C. Yan, Z. Li, and Z. Shao, "Flexible silicon solar cells with high power-to-weight ratios," *Nature*, vol. 626, pp. 105–110, Jan. 2024. [Online]. Available: https://doi.org/10.1038/s41586-023-06948-y

[6] A. Karim, A. F. M. A. U. Sheikh, S. A. Chowdhury, and M. H. Chowdhury, "Optimizing the Parameters of Core-Shell Nanoparticles with Different Algorithms to Enhance Performance of Thin-Film Solar Cells," in *2024 International Conference on Advances in Computing, Communication, Electrical, and Smart Systems (iCACCESS)*, Mar. 2024, pp. 1–6. [Online]. Available: https://ieeexplore.ieee.org/document/10499492

[7] H. I. Park, S. Lee, J. M. Lee, S. A. Nam, T. Jeon, S. W. Han, and S. O. Kim, "High Performance Organic Photovoltaics with Plasmonic-Coupled Metal Nanoparticle Clusters," *ACS Nano*, vol. 8, no. 10, pp. 10 305–10 312, Oct. 2014, publisher: American Chemical Society. [Online]. Available: https://doi.org/10.1021/nn503508p

[8] C. Farcau, N. M. Sangeetha, N. Decorde, S. Astilean, and L. Ressier, "Microarrays of gold nanoparticle clusters fabricated by Stop&Go convective self-assembly for SERS-based sensor chips," *Nanoscale*, vol. 4, no. 24, pp. 7870–7877, Nov. 2012, publisher: The Royal Society of Chemistry. [Online]. Available: https://doi.org/10.1039/C2NR32781C

[9] O. J. H. Chai, Z. Liu, T. Chen, and J. Xie, "Engineering ultrasmall metal nanoclusters for photocatalytic and electrocatalytic applications," *Nanoscale*, vol. 11, no. 43, pp. 20 437–20 448, Nov. 2019, publisher: The Royal Society of Chemistry. [Online]. Available: https://doi.org/10.1039/C9NR07272A

[10] "Solar cell methodology - Ansys Optics." [Online]. Available: https://optics.ansys.com/hc/en-us/articles/360042165634-Solar-cell-methodology

[11] J. S. C. Prentice, "Computer simulation of the effect of phosphorous doping of the i-layer in a thin-film a-Si:H p-i-n solar cell," *Solar Energy Materials and Solar Cells*, vol. 61, no. 3, pp. 287–300, Mar. 2000. [Online]. Available: https://doi.org/10.1016/S0927-0248(99)00116-6

[12] "Planar silicon solar cell." [Online]. Available: https://optics.ansys.com/hc/en-us/articles/360042165534-Planar-silicon-solar-cell

[13] J. Kennedy and R. Eberhart, "Particle swarm optimization," in *Proceedings of ICNN'95 - International Conference on Neural Networks*, vol. 4, Nov. 1995, pp. 1942–1948 vol.4. [Online]. Available: https://ieeexplore.ieee.org/document/488968

[14] A. J. Haque, M. Shaky, S. Hasan, T. Ahmed Khan, M. Kaiser, and M. Chowdhury, "Use of Genetic Algorithm and Finite-Difference Time-Domain Calculations to Optimize Plasmonic Thin-Film Solar Cell Performance," Jun. 2023, pp. 459–472.

[15] R. B. Sultan, A. A. Suny, M. H. Hossain, T. Noor, and M. H. Chowdhury, "Particle Swarm Optimization for Performance Enhancement of Cadmium Telluride Thin Film Solar Cells by Embedded Nano-Grating Structures with a Plasmonic Metal Coating Layer," Rochester, NY, Jun. 2024. [Online]. Available: https://doi.org/10.1016/j.heliyon.2024.e38775

[16] "Optimization utility Ansys Optics." [Online]. Available: https://optics.ansys.com/hc/en-us/articles/360034922953-Optimization-utility

[17] H.-N. Barad, H. Kwon, M. Alarcón-Correa, and P. Fischer, "Large Area Patterning of Nanoparticles and Nanostructures: Current Status and Future Prospects," *ACS Nano*, vol. 15, no. 4, pp. 5861–5875, Apr. 2021, publisher: American Chemical Society. [Online]. Available: https://doi.org/10.1021/acsnano.0c09999

[18] S. Jambhulkar, D. Ravichandran, Y. Zhu, V. Thippanna, A. Ramanathan, D. Patil, N. Fonseca, S. Thummalapalli, B. Sundaravadivelan, A. Sun, W. Xu, S. Yang, A. Kannan, Y. Golan, J. Lancaster, L. Chen, E. Joyee, and K. Song, "Nanoparticle Assembly: From Self Organization to Controlled Micropatterning for Enhanced Functionalities," *Small*, vol. 20, p. e2306394, Sep. 2023. [Online]. Available: https://doi.org/10.1002/smll.202306394

[19] J. Martin and J. Plain, "Fabrication of aluminium nanostructures for plasmonics," *Journal of Physics D: Applied Physics*, vol. 48, Dec. 2014. [Online]. Available: https://dx.doi.org/10.1088/0022-3727/48/18/184002

[20] A. J. Haque, M. A. Suny, R. Sultan, T. Ahmed Khan, and M. Chowdhury, "Effects of defective plasmonic metal nanoparticle arrays on the opto-electronic performance of thin-film solar cells: computational study," *Applied Optics*, vol. 62, Apr. 2023. [Online]. Available: https://doi.org/10.1364/AO.485633